A Theoretical Study on the Catalytic Synergetic Effects of Pt/Graphene Nanocomposites

Wu Qin and Xin Li*

Department of Chemistry, Harbin Institute of Technology, Harbin 150090, P. R. China

Received: August 2, 2010; Revised Manuscript Received: September 11, 2010

A detailed understanding of synergetic catalytic effect of graphene−metallic nanoparticles composite is challenging and the heart of the graphene-based catalyst. On the basis of density functional theory, we have theoretically studied the confinement of Pt/graphene composite by using the conversion from the ozone decomposition to the hydroxyl radical generation as the probe reactions, finding that graphene plays a direct role in regulating the electronic structure of the Pt nanoparticles during every step of reactions. Furthermore, an electric field was introduced to guide the charge transfer direction between the Pt nanoparticles and the graphene sheet and to change the electronic state of the Pt/graphene composite. We attribute the presenting synergetic catalytic effect to the transfer of electrons between the π orbitals of graphene and the d orbitals of metal atoms. We believe that our discovery may be of a quite general nature and could lead to new advances and development of a new class of graphene-based catalyst.

1. Introduction

Graphene, with a well-defined, two-dimensional, honeycomb structure of carbon atoms, boasts some very special characteristics, such as extreme tear-resistance, excellent thermal conductivity, ductility, and unusual electronic properties.[1−10] This attracts great attention in basic research,[11−16] microelectronics,[3,17,18] large-area optoelectronics,[19−21] sensors,[22−24] and actuators.[25] By supporting transition-metal catalyst particles on graphene sheets, it should be possible to impart to the material particular electronic characteristics. For these reasons, intensive research is being conducted worldwide into the synthesis and characterization of graphene-based materials for catalytic, magnetic, and optoelectronic applications.[26−38] In the area of catalysis, the graphene sheets decorated by metal or metal oxide nanoparticles have been prepared for applications. TiO_2/graphene composites were successfully synthesized, and experiments under different conditions demonstrated that graphene is a very promising candidate for development of high-performance catalysts.[39,40] Graphene sheets decorated by Pt nanoparticles have been prepared, and their catalytic activity has been investigated by experiments that show that the Pt/graphene composites could act as excellent catalysts in electrocatalysis and fuel cells.[41−44] These experiments show that such 2-D sheets with a large area of carbon surface could anchor catalyst particles without aggregation and act as an electronic communicating platform between metal or metal oxide nanoparticles anchored on the graphene sheet. These findings pave the way for the development of novel catalyst systems. However, the present understanding is not satisfactory to predict relationships between graphene sheet and metal or metal oxide nanoparticles, especially the synergetic catalytic effect of such graphene-based catalyst for applications to modulate the catalytic reactions in a controlled fashion. Therefore, further investigation of metal or metal oxide nanoparticles supported on graphene sheets is highly desirable.

In this investigation, based on density functional theory (DFT) calculations, reactions related to the conversion from the ozone decomposition to the hydroxyl radical generation, which are critically important reaction processes in the environmental field, were used as the probe reactions to investigate the synergetic effect of Pt/graphene composite. An electric field was introduced to guide the charge transfer direction between the Pt nanoparticle and the graphene sheet and to change the electronic state of the Pt/graphene composite, to further detect the synergetic effect of graphene on the Pt nanoparticle. We would like to highlight such a synergetic effect between graphene and the catalyst nanoparticles and its influence for the catalytic performances, which has not been investigated before in catalysis involving graphene sheets. This discovery can show a quite general nature of Pt/graphene nanocomposites, which will favor the application of graphene-based composite materials and development of new catalysts.

2. Computational Methods

All calculations are performed using density functional theory (DFT) with generalized gradient approximation (GGA) for exchange correlation potential and Perdew−Burke−Ernzerholf (PBE) functional.[45,46] To simulate the synergetic effect of Pt supported on graphene, the following procedure is used. A graphene sheet containing 84 carbon atoms (the edge is terminated by 24 hydrogen atoms) was selected as the supporter. The monolayer Pt cluster can be obtained by cleaving the surface along the Pt crystal (100) surface based on the (2×2) surface unit cell and then removing the periodic condition of the single layer plane. Then a Pt cluster with nine atoms was obtained from the open (100) surface, since the well-defined (100) facets on Pt nanoparticle surfaces make the Pt nanoparticles an ideal material for understanding the influence of nanocrystal facets on catalytic performance.[47,48] When we optimized the Pt/graphene composite, atoms of both the graphene sheet and the Pt cluster were allowed to relax freely. Second, after optimizing the Pt/graphene composite, we investigated the nature of the contact of graphene with Pt nanoparticles and the synergetic effect of such a Pt/graphene composite by using the probe reactions related to the conversion from the ozone decomposition to the hydroxyl radical generation. We discussed the ozone

* To whom correspondence should be addressed. E-mail: lixin@hit.edu.cn.

10.1021/jp1072523

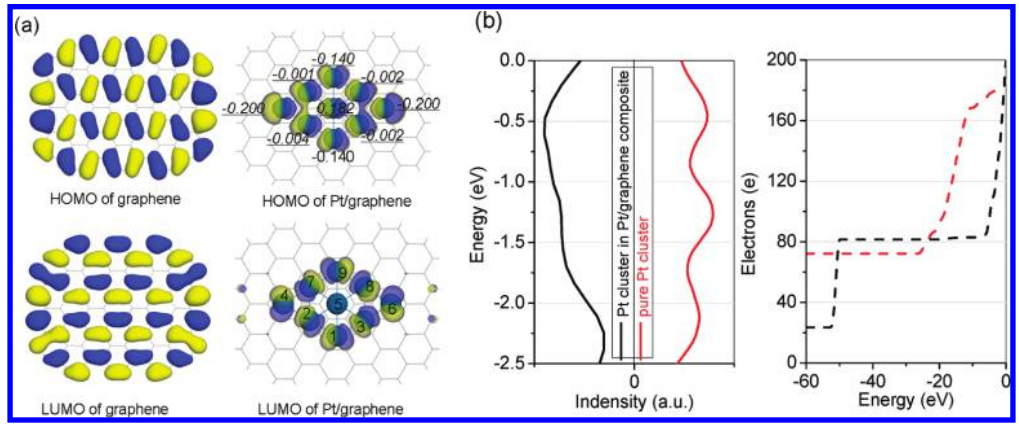

Figure 1. (a) The optimized structure of the graphene sheet and Pt/graphene composite with the isosurface (0.01) of the highest occupied molecular orbital (HOMO) and the lowest unoccupied molecular orbital (LUMO). The value of the partial Mulliken charge is underlined. (b) Total density of states of the Pt cluster and its integrogram.

molecule decomposition and the generation of hydroxyl radical on the surface of such a Pt/graphene composite.

To further study the synergetic catalytic behaviors of Pt/graphene composite, electric fields with field intensities of ±0.136 and ±0.054 eV were applied perpendicular to the graphene plane, in the positive *Z* direction (defined as "+") or the opposite *Z* direction (defined as "−").

Prior to calculating the generation of hydroxyl radical, we examined the interaction between ozone molecules and Pt cluster surfaces to determine the adsorption configurations of ozone−Pt/graphene systems with the lowest energy. Then, the transition states for the hydroxyl radical generation reaction on Pt/graphene surfaces were investigated using DFT combined with a new formulation of the linear (LST) and quadratic synchronous transit (QST) methods.[49]

3. Results and Discussion

3.1. Property of Pt/Graphene Composite. The unique electronic property and geometric structure of each kind of catalyst contribute to its activity and behavior in the catalytic reaction. Here, to theoretically analyze the electronic property of the Pt/graphene composite, we investigated the interaction of Pt cluster with graphene sheet by approaching the Pt cluster to the surface of the graphene sheet with the largest interaction area. Figure 1 illustrates the optimized structure of graphene sheet and Pt/graphene composite with the isosurface of the highest occupied molecular orbital (HOMO) and the lowest unoccupied molecular orbital (LUMO). The graphene is an explanate, two-dimensional sheet, and the graphene hexagon has a C−C bond length of 1.420 Å, corresponding to the results reported previously.[50] In the Pt/graphene composite, the interaction from Pt atoms led to a relaxation (7.38%) to the graphene sheet along the *Z* direction. As seen in Figure 1, the HOMO and LUMO of the graphene sheet are widely delocalized over the graphene surface, which indicates that both hole and excess electron can move widely on the normal graphene surface. The HOMO and LUMO of the Pt/graphene composite show the trend of localization at Pt atoms with partial electronic density transfer from the graphene sheet to the Pt cluster, for which we calculated the Mulliken charge population of the nine Pt atoms of the Pt/graphene composite. The atomic charges for Pt-4 and Pt-6 are −0.200, which possess the highest electron density. Pt-5 possesses the least electron density, which shows to be +0.182. According to the Mulliken charge population calculation, 0.479 e transferred from the graphene sheet to the Pt cluster. This is the quantum-trapping effect analyzed by the recent study of Sun et al.,[51] who proposed the bond order−length−strength (BOLS) correlation theory[52,53] for the quantitative analysis of the catalytic behavior of the undercoordinated atoms. The Pt atom has been identified as an acceptor in the catalytic reactions because of quantum trapping depression. The excess electronic charge coming from substrate can reduce interface impedance for the electron transfer process and promote an electron-withdrawing reaction on the surface.

The total electron density of states (DOS) of the Pt cluster is shown in Figure 1b. In Figure 1b, the total DOS is plotted in arbitrary units vs the energy for the Pt cluster in the Pt/graphene composite (black line) and for comparison for the pure Pt cluster (red line). For the Pt cluster in the Pt/graphene composite, more states are found at energies close to the Fermi level, while they are much lower for the pure Pt cluster, as shown in the integrogram on the left of Figure 1b. Obviously, the total DOS of the Pt cluster in the Pt/graphene composite with its high-lying states allows for an energetically easier excitation and renders the Pt cluster thereby more reactive than the pure Pt cluster.

3.2. Decomposition of Ozone on the Surface of Pt/Graphene Composite. Catalytic reactions from ozone decomposition to the hydroxyl radical generation were used as probe reactions to investigate the catalytic behaviors of Pt/graphene composite. As the first step to initiate reactions, we investigate the interaction between ozone and catalyst. Orientation alignment is important to the surface interaction between the atoms of sorbate and sorbent. In our calculation, the LUMO of the optimized ozone molecule relates to the two π^* antibonding molecular orbitals (MOs) of the ozone molecule. The LUMO and the HOMO of the Pt/graphene composite, as shown in Figure 1a, relates to 5d orbital of Pt atom. Hence, the interaction between ozone and Pt/graphene composites will happen to the 2p orbit of ozone and the 5d orbital of Pt atom. In addition, ozone usually acts as an electron acceptor, which will favor attack on the Pt atom that has sufficient electron density to facilitate donation from the metal d_{xz} orbital to the π^* molecular orbital from an O atom of the ozone molecule. The interaction of ozone molecule with the surface of Pt/graphene composite was done by approaching the ozone molecule to the Pt-4 in the favorite p−d overlap direction. As comparison, we also investigated the adsorption of ozone to Pt-5 of the Pt/graphene composite.

When ozone molecule interacted with Pt-4 or Pt-5, the ozone molecule decomposed into an atomic oxygen species and an

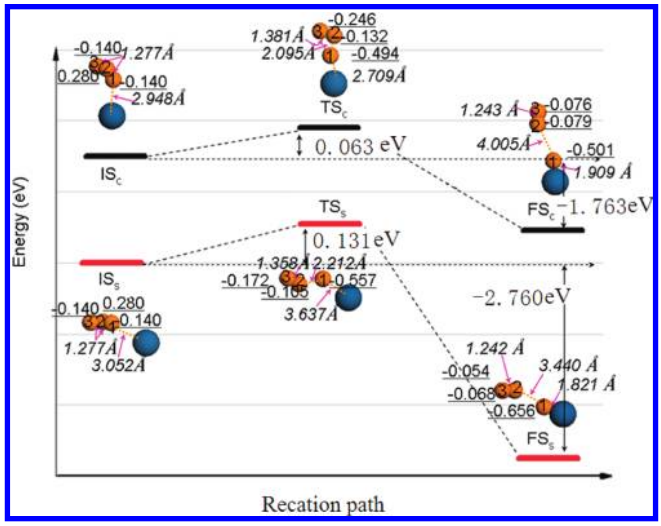

Figure 2. Calculated potential energy profiles given in eV for the decomposition of the ozone molecule over Pt-4 and Pt-5 of the Pt/graphene composite. Distances are given in units of angstroms. Charges of the atoms are underlined. The IS_s, TS_s, and FS_s denote the initial state, transition state, and final state for the reaction over Pt-4, respectively. The IS_c, TS_c, and FS_c denote the initial state, transition state, and final state for the reaction over Pt-5, respectively. A yellow ball is an oxygen atom, and a blue ball is a platinum atom.

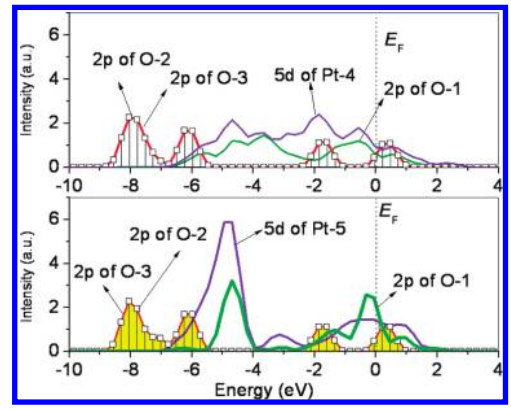

Figure 3. Partial DOS of the atomic oxygen, and the oxygen atom of oxygen molecule for the adsorption configurations. The upper panel corresponds to FS_s in Figure 2. The lower panel corresponds to FS_c in Figure 2. The vertical black dotted line indicates the Fermi level (E_F = 0.000 eV).

oxygen molecule. Figure 2 shows the calculated potential energy profiles for the decomposition of the ozone molecule adsorbed to the Pt-4 and Pt-5 of the Pt/graphene composite. The reactions initiate from the optimized physisorption geometries of the O_3 adsorption to the Pt-4 and Pt-5 of the Pt/graphene composite, respectively. The final states correspond to the chemisorption of ozone molecule over Pt-4 and Pt-5 of the Pt/graphene system. As seen in Figure 2, the ozone molecule on Pt-4 decomposed into an atomic oxygen species and an oxygen molecule. The atomic oxygen species is chemically adsorbed on Pt-4 with a distance of 1.821 Å and shows a distance of 3.440 Å to the oxygen molecule, which verified the break of one O−O of the ozone molecule on the catalyst surface. Ozone molecule also decomposed into an atomic oxygen species and O−O group while interacted with the Pt-5 of the Pt/graphene composite. The atomic oxygen species chemically bonds to the Pt-5 with a distance of 1.909 Å and shows a distance of 4.005 Å to the oxygen molecule. The overlap (0.521) between the atomic oxygen species and Pt-4 is larger than the overlap (0.384) between the atomic oxygen species and Pt-5. The ozone decomposition reactions related to the Pt-4 and Pt-5 were found to be exothermic by 2.760 and 1.763 eV with barrier energies of 0.131 and 0.063 eV, respectively. We found that both of the decomposition reactions of ozone molecule on the Pt-4 and Pt-5 occur easily. However, the side channel related to Pt-5 is more accessible than the center channel (related to Pt-4), and this may correspond to the energy difference between the outermost orbit of the Pt atom and the LUMO of the ozone molecule, where the difference between the outermost orbit of Pt-5 and the LUMO of the ozone molecule should be less than that between Pt-4 and the ozone molecule. According to the calculated reaction energy (E_r), the adsorption of ozone molecule on Pt-4 is stronger than on Pt-5.

We further analyzed the atomic charge distribution of the system at the initial state, transition state, and final state of the reaction. During the ozone decomposition reaction at the Pt-4 site, 0.812 e transferred from the graphene to the Pt cluster, and then 0.778 e transferred to the adsorbed ozone molecule, which activated the ozone molecule, leading to the breaking of one O−O bond of the ozone and the strengthening of the other O−O bond. During the ozone decomposition reaction at the Pt-5 site, with partial electron density transferring to the adsorbed ozone molecule, atomic charge repopulated in the Pt/graphene composite, where the Pt cluster possessed excess electron density (−0.034). Though only 0.586 e transferred from the graphene to the Pt cluster, 0.656 e transferred to the adsorbed ozone molecule, leading to the decomposition of the ozone. As a result of the ozone decomposition reaction at Pt-5 site, the Pt cluster became cationic with a slightly positive charge of 0.070. Comparing the two reaction channels, we can observe that more electron density transferred from the graphene to the Pt cluster, and then there is 0.122 e more transferring to the ozone molecule adsorbed to Pt-4 than to Pt-5, which once again verified that there was further interaction between the graphene layer and the Pt cluster during the decomposition of ozone molecule through the reaction.

To further understand the decomposition of ozone molecule on the Pt/graphene composites, we calculated the partial density of states (PDOS) of the Pt atom of the Pt/graphene composite, the atomic oxygen, and the oxygen atom of oxygen molecule for the final state configurations, where the PDOS of Pt-4 and Pt-5 were also given, as shown in Figure 3. For the ozone adsorption to Pt-4 in Figure 2, the PDOS of O-2 and O-3 overlapped in the four energy regions around −8.000, −6.000, −1.500, and 0.500 eV, since O-2 and O-3 in the oxygen molecule show almost the same electronic properties. However, the PDOS of O-1 differed greatly to that of O-2 or O-3. The atomic oxygen O-1 shows its density of states from −6.000 to −2.000 eV and −2.000 to 2.000 eV. O-1 and Pt-4 hybridize mainly via the Pt-5d orbital and the O-2 p orbital, and −6.000 to −2.000 eV related to the π MO formed by electronic interaction between the 2p orbit of the atomic oxygen and the $5d_{xy}$ orbit of Pt, where electron transferred from the HOMO of Pt atom to the LUMO of O-1. In contrast, −2.000 to 2.000 eV is related to the π^* antibonding MO formed by the 2p orbit of O-1 and the $5d_{yz}$ orbit of the Pt atom. For the ozone adsorption to Pt-5 in Figure 2, the PDOS of O-2 and O-3 are almost the same as those in the adsorption system in which ozone interacts with Pt-4 of the Pt/graphene composite, showing their main peaks at the ranges of around −8.000, −6.000, −1.500, and 0.500 eV. The PDOS of O-1 are shown to be localized from −5.500 to 4.000 eV and −2.000 to 1.000 eV, while the 2p electrons of the O-1 bonding to Pt-4 delocalized in a large range from −6.500 to 1.000 eV. This difference can be explained as

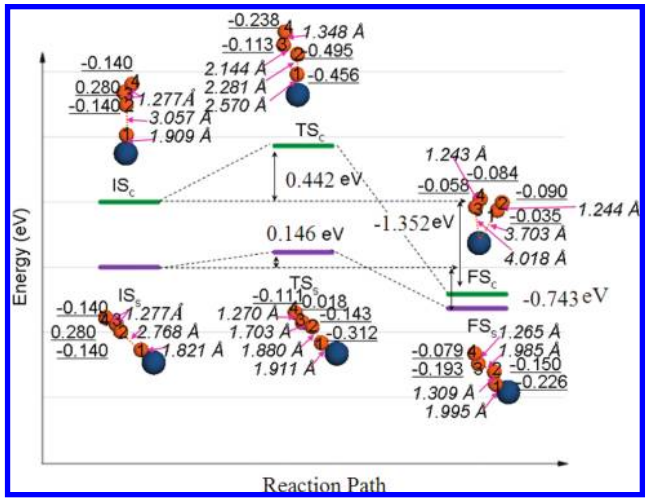

Figure 4. Energy profiles for the reaction between the atomic oxygen species and another ozone molecule over Pt-4 and Pt-5. Distances are given in units of angstroms. Charges of the atoms are underlined. The IS_s, TS_s, and FS_s denote the initial state, transition state, and final state for the reaction over Pt-4, respectively. The IS_c, TS_c, and FS_c denote the initial state, transition state, and final state for the reaction over Pt-5, respectively. A yellow ball is an oxygen atom, and a blue ball is a platinum atom.

the 2p orbital of the O-1 bonding to Pt-4 being affected more strongly by the Pt cluster than that of the O-1 bonding to Pt-5. Comparing the PDOS of O-1, Pt-4, and Pt-5 in Figure 3, it can be observed that the atomic oxygen species is chemisorbed to Pt-4 and Pt-5, respectively.

3.3. Generation of Superoxide Species. In our calculation, the atomic oxygen species cannot interact with the water molecule directly; hence, we focused on another ozone molecule interacting with the atomic oxygen species on the Pt/graphene composite. Using the total energy minimization technique, when another ozone molecule interacted with the atomic species on Pt/graphene composite, the ozone molecule decomposed, leading to the generation of an oxygen molecule and superoxide species. Figure 4 shows the energy profiles for the generation of an oxygen molecule and superoxide species over Pt-4 and Pt-5. When interacting with the atomic oxygen species over Pt-4, the ozone molecule decomposed and bonded to the atomic oxygen species to generate an oxygen molecule and a superoxide species. This process is exothermic by 0.632 eV, and the barrier energy is 0.146 eV, which shows that this reaction can occur easily. The superoxide species shows a bond length of 1.309 Å, which is larger than that of the pure oxygen molecule (1.210 Å) and more similar to that of the free superoxide (O_2^-) anion (1.34 Å calculated previously;[54] 1.33 Å in Huang's work[55]). In addition, according to the Mulliken atomic charge population calculation results, there was 0.376 e transfer from Pt/graphene composite to the superoxide species, while 0.272 e transfer to the O-3−O-4 group. The superoxide species formed on Pt/graphene composite will play a more important role in the following reaction to water molecule, which will be further discussed below.

However, when another ozone molecule interacted with the atomic oxygen species adsorbed on Pt-5 on the Pt/graphene composite, two oxygen molecules are generated. In this process, the reaction energy is −1.415 eV and the barrier energy is 0.442 eV. As shown in Figure 4, bond lengths for the two oxygen molecules are 1.243 and 1.244 Å, respectively, which is similar to that of the pure oxygen molecule. Furthermore, Mulliken population analysis showed that there was only 0.220 e transferring to the four oxygen atoms. Hence, it can also be observed in the second step that further electronic interaction happened between graphene and the Pt cluster: 0.803 e transferred from graphene to the Pt cluster and then 0.648 e to the surface reactants over Pt-4, and 0.542 e transferred from graphene to the Pt cluster and then 0.267 e to the surface reactants over Pt-5. The electron transfer from graphene to the Pt cluster also played an important role in the generation of superoxide radical, which superoxide species cannot generate over Pt-5.

Furthermore, Figure 5a shows the PDOS of O-1−O-2 and O-3−O-4 in the systems in which the ozone molecule interacted with the atomic oxygen species bonding to Pt-4 of Pt/graphene composite (FS_s in Figure 4). As observed in Figure 5a, there are two main regions with high electron density for the 2p orbital of O-1−O-2, which are around −15.000 eV and at the range from −9.000 to −5.000 eV below the Fermi level, corresponding to the bonding states of O-1−O-2. The antibonding state is around −2.000 to 1.000 eV, which is largely occupied. There is certain hybridization between the 2s and 2p orbitals of the oxygen atom. While comparing to the PDOS for the pure O_2, we can observe that the electronic interaction and charge transfer give rise to the change and enhancement of the PDOS of O-1−O-2, resulting in the strong activity of the O-1−O-2 superoxide group. Though there is a left move relative to the PDOS of $•O_2^-$, the PDOS of O-1−O-2 is almost similar to that of $•O_2^-$, which will prefer to act as $•O_2^-$ during the complex oxidation processes. However, the PDOS of the active oxygen species O-3−O-4 shows some difference compared to that of O-1−O-2. As shown in Figure 5a, the 2s PDOS of O-3−O-4 at around −16.000 to −13.000 eV is opposite to that of O-1−O-2, and the peak at around −6.000 eV for 2p below the Fermi level is sharper than that of O-1−O-2, which indicates that 2p electrons of O-3−O-4 are more likely to fill at around −6.000 eV, while 2p electrons of O-1−O-2 delocalized in a large range from −9.000 to −5.000 eV. The PDOS of O-3−O-4 is also different from that of the pure O_2 and $•O_2^-$, possessing more electron density than that of the pure O_2 and less than that of $•O_2^-$. We take the O-3−O-4 group as an intermediate between O_2 and $•O_2^-$. If further interacting with the surface of catalyst can transfer more electronic charge from Pt/graphene to the O-3−O-4 group, the O-3−O-4 group can also act as an active oxygen molecule species. As comparison, we have calculated the PDOS of O-1−O-2 and O-3−O-4 in the interaction systems in which the ozone molecule are interacting with the atomic oxygen species bonding to Pt-4 on the Pt/graphene composite (Figure 4), as shown in Figure 5b. It can be observed that the PDOS of O-1−O-2 on the surface of the Pt/graphene composite is almost the same as that of O-3−O-4, which shows little difference to that of the pure O_2, except for a left shift due to the partial electron density transfer from catalyst surface to the four oxygen atoms. These results further verified that O-1−O-2 and O-3−O-4 in the interaction systems are free oxygen molecules.

3.4. Generation of Hydroxyl Radical. We further investigated that two water molecules interacted with the two active oxygen groups over the Pt-4 site on the Pt/graphene composite; the results are shown in Figure 6. The geometrical feature shows that the water molecules approached the superoxide species O-1−O-2 and decomposed into OH and OOH groups. The bond length of the OH group is 0.985 Å, which shows a distance of 2.025 Å to the Pt-4 atom. A hydrogen bond with 1.588 Å was formed between the OH and OOH groups. For the OOH group, the O−O bond length is 1.444 Å and the O−H bond length is

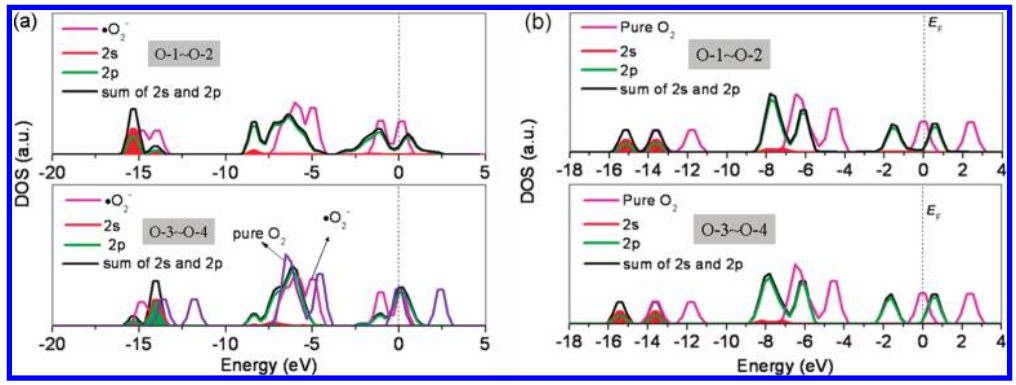

Figure 5. PDOS of O-1−O-2 and O-3−O-4 in the interaction systems in which another ozone molecule is interacting with the atomic oxygen species bonding to Pt-4 on the Pt/graphene composite (a) and to the atomic oxygen species bonding to Pt-5 on the Pt/graphene composite (b). The vertical black dotted line indicate the Fermi level (E_F = 0.000 eV).

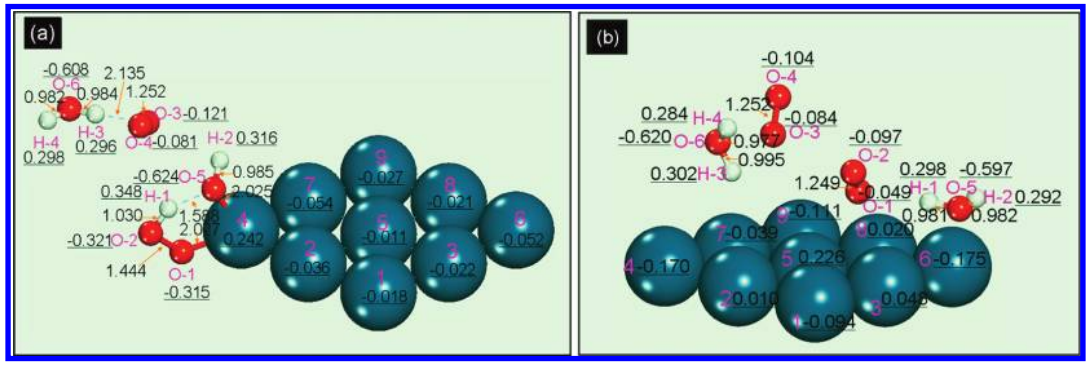

Figure 6. Optimized stable structures for the interaction between the two water molecules and the two active oxygen groups related to (a) the Pt-4 site and (b) the Pt-5 of the Pt/graphene composite. Distances are given in units of angstroms. Partial Mulliken atomic charge distributions are underlined. A red ball is an oxygen atom, a white ball is a hydrogen atom, and a blue ball is a platinum atom.

1.030 Å. The OOH group shows its distance to the Pt-4 atom to be 2.027 Å shorter than that of the superoxide species adsorbed to the Pt-4 atom (Figure 4). The interaction between the other water molecule and the O-3−O-4 group is relatively moderate. The bond length of O-3−O-4 is 1.252 Å, which shows little change compared to that in Figure 4. The two bond lengths of O−H in the second water molecule are almost equal to each other, which maintains the equilibrium of the water molecule. The distance between the water molecule and the O-3−O-4 group is 2.135 Å, which is large enough to prevent the formation of a chemical bond. According to the Mulliken atomic charge distribution, 0.812 e transferred from the graphene sheet and then a partial electronic charge appears on the upper surface reactants. As can be seen in Figure 6a, electronic interaction and charge repopulation happened between the superoxide species and the water molecule and led to the decomposition of the water molecule and the generation of the OH and OOH groups, while no obvious electronic interaction happened between the O-3−O-4 group and the other water molecule. For comparison, we also introduce two water molecules to interact with the two O−O groups related to Pt-5 in the configuration shown in Figure 4, the result of which is shown in Figure 6b. It is observed that the two oxygen molecules O-1−O-2 and O-3−O-4 show their bond length of 1.249 and 1.252 Å, respectively. The bonds for H-1−O-5 and O-5−H-2 are 0.981 and 0.982 Å, respectively, which is in its balanced state. However, in the other water molecule H-3−O-6−H-4, one bond length is 0.995 Å and the other 0.977 Å. The lengthening of H-3−O-6 is due to the slight electronic interaction between the H-3 and the surface of the Pt cluster. Mulliken atomic charge population also shows that electronic charges in the water molecules and the oxygen molecules are almost kept in balance.

Figure 7a lists the PDOS of Pt-4 and the total DOS of the O-1−O-2 group, the O-3−O-4 group, and the OH group of Figure 6a. The total DOS of the O-3−O-4 group is consistent with that of the pure O_2, as shown in Figure 5b, which implies that the O-3−O-4 group became a free oxygen molecule with the release of its partial electronic charge after interacting with a water molecule in the aqueous solution. The total DOS of the O-1−O-2 group lies from −9.000 to 1.000 eV with another peak at around −16.000 eV. The wide delocalization in the range from −9.000 to 1.000 eV is due to the formation of the OOH group, which will act as an active species during the catalytic oxidation reaction. The total DOS of the OH group delocalized in the broad range from −9.000 to 1.000 eV. The 2p orbital of O-5 in the OH group hybridized with the 5d orbital of Pt-4, which implies that the OH group is chemisorbed to the Pt-4. Comparing the DOS of the O-1−O-2 group and the O-3−O-4 group to those before interacting with water molecules (Figure 5a) shows that the O-3−O-4 group becomes a free oxygen molecule released in the aqueous solution with release of the partial redundant negative charge, and the formation of the OOH group makes itself more active than the O-1−O-2 group with the delocalization of the outer-shell electron in a more broad energy range. Figure 7b shows the total DOS of the O-1−O-2 group and the O-3−O-4 group of Figure 6b, which are almost the same as that of the pure O_2. The DOS of the O-1−O-2 and O-3−O-4 groups of Figure 6b further verifies that the O-1−O-2 and O-3−O-4 groups are free oxygen molecules, which cannot react with water molecule to form active radicals.

3.5. Electric Field Effect on the Activity of Pt/Graphene Composite. We further detect the synergetic catalytic effect of the Pt/graphene composite in an electric field. We introduced the

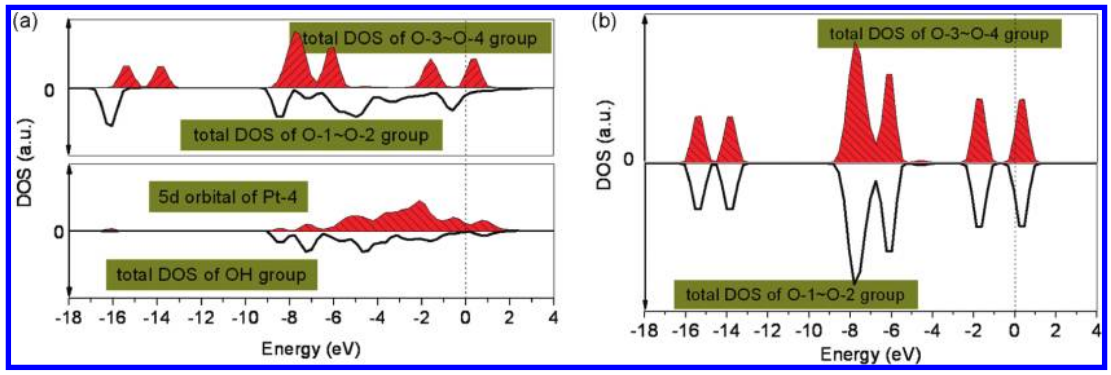

Figure 7. (a) PDOS of Pt-4, the total DOS of the O-1−O-2, O-3−O-4, and OH groups of Figure 6a; (b) the total DOS of the O-1−O-2 and O-3−O-4 groups of Figure 6b. The vertical black dotted line indicates the Fermi level (E_F = 0.000 eV).

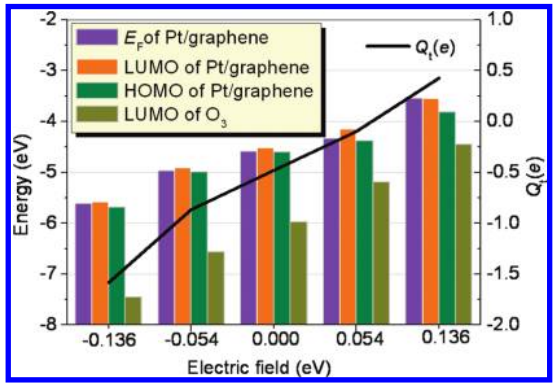

Figure 8. Left-hand scale: E_F, HOMO, and LUMO of Pt/graphene and LUMO of O_3. Right-hand scale: Charge transfer (Q_t) between the graphene layer and the Pt cluster.

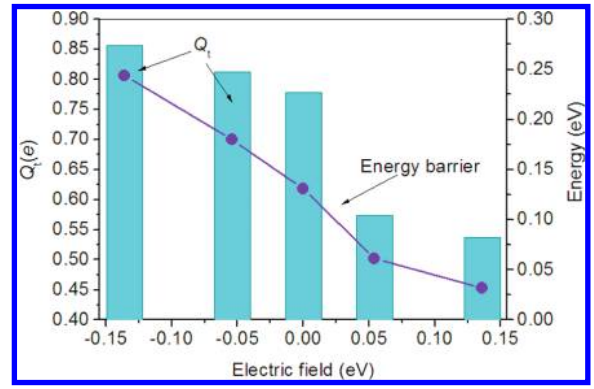

Figure 9. Barrier energy for the decomposition of ozone molecule on Pt/graphene and the electron transfer from Pt/graphene to the adsorbate under different electric fields.

electric field with different field intensities of −0.136, −0.054, 0.000, 0.054, and 0.136 eV, to investigate its effect on the change of electronic properties of the Pt/graphene system, which will therefore affect the catalytic reaction on the surface. The strong electrostatic-field-effect modulation of the Pt/graphene composite was determined by the frontier molecular orbital (FMO) analysis. Figure 8 shows the energies of the HOMO and LUMO of the Pt/graphene system, which suggests that the energies of the HOMO, LUMO, and E_F increase with the increase of field. The band gap between the HOMO and LUMO of Pt/graphene under a field of −0.136, −0.054, 0.000, 0.054, and 0.136 eV is 0.097, 0.081, 0.072, 0.233, and 0.265 eV, respectively. In the comparison to the energy of the HOMO and LUMO of Pt/graphene, it was found that the highest energy value of the HOMO and the largest band gap were obtained at 0.136 eV. In Figure 8, it can be observed that Q_t is −1.580, −0.865, −0.479, −0.100, and 0.429 for the Pt/graphene composite at a field of −0.136, −0.054, 0.000, 0.054, and 0.136 eV, respectively. The curve in Figure 8 shows that the relation between Q_t and the field is almost linear. The increase of field density in the opposite Z direction led to more electrons being transferred from the graphene to the Pt cluster, which made the Pt cluster an anion [$(Pt9)^{x-}$]. On the contrary, while the electric field increased in the Z direction, the Pt cluster became a cation [$(Pt9)^{x+}$], where charge transferred from the Pt atoms to the graphene. The modulation related to charge transfer between graphene and Pt atoms verified that the Pt/graphene composite is a system of efficient integrality with special electronic properties differing from the simple addition of Pt particle and graphene sheet.

While ozone adsorbed to the surface of the Pt/graphene system, an interaction happened between the HOMO of the Pt/graphene composite and the LUMO of the adsorbed ozone molecule. Accordingly, it is feasible to adopt the LUMO energies of the ozone molecule to characterize their Lewis acidity and the HOMO energies of the Pt/graphene composite to characterize their Lewis basicity. The energy gaps between the two orbits can be used to predict how the Pt/graphene composite interacts with ozone molecule; see the equation below

$$E_{\mathrm{LUMO-HOMO}} = E_{\mathrm{LUMO}}(\mathrm{ozone}) - E_{\mathrm{HOMO}}(\mathrm{Pt/graphene}) \quad (1)$$

where E_{LUMO}(ozone) and E_{HOMO}(Pt/graphene) refer to the LUMO energy of the ozone molecule and the HOMO energy of the Pt/graphene composite, respectively. In the O_3−Pt/graphene system, the $E_{\mathrm{LUMO-HOMO}}$ is −1.769, −1.570, −1.374, −0.816, and −0.639 eV under a field of −0.136, −0.054, 0.000, 0.054, and 0.136 eV, respectively. The $E_{\mathrm{LUMO-HOMO}}$ decreases with the increase of field in the Z direction. Smaller energy gaps favor electrons transfer from the HOMO of Pt atoms to the LUMO of the ozone molecules, hence promoting the ozone decomposition reaction. Figure 9 shows the barrier energy for the decomposition of the ozone molecule on Pt/graphene and the electron transfer from Pt/graphene to the sorbate under different electric fields. The barrier energies for the reactions under a field of −0.136, −0.054, 0.000, 0.054, and 0.136 eV are 0.244, 0.180, 0.131, 0.061, and 0.032 eV, respectively. We found that the barrier energy decreased with the increase of fields, corresponding to the calculated $E_{\mathrm{LUMO-HOMO}}$. Q_t is 0.856, 0.812, 0.778, 0.574, and 0.537 under a field of −0.136, −0.054, 0.000, 0.054, and 0.136 eV, respectively. Electron transfer from Pt/graphene to the sorbate decreased with the increase of electric field. Hence, according to the analysis above corresponding to the generation of superoxide species and hydroxyl radical, though the positive electric field accelerates the decomposition of the ozone molecule, the negative electric field favors the next steps relating to the generation of superoxide species and hydroxyl radical.

According to the calculations for the presence of electric field, the delocalization of the electrons between the π orbitals of graphene and the d orbitals of the metal atoms affected the reactions converting from the ozone decomposition to the hydroxyl radical generation. The modulation effect of the electric field for the electronic structures and the physicochemical properties of Pt/graphene composite verified the synergetic catalytic effect of the Pt/graphene composite.

4. Conclusions

Electronic properties of Pt/graphene composite and its synergetic effect for reactions were investigated using DFT calculation. When Pt particles were supported on graphene, an electronic interaction occurred between Pt atoms and the graphene, leading to electron transfer from graphene to Pt atoms. Further electron transfer can be observed during further catalytic reactions on the surface of Pt/graphene composite, including the ozone decomposition reaction, supperoxide radical generation reaction, and hydroxyl radial generation reaction. These results demonstrate that graphene not only acts as a supporter and stabilizer, but also plays a direct role in regulating the electronic structure of the Pt nanoparticle during reactions. An electric field effect can guide charge transfer between graphene and Pt nanoparticle and change the electronic state of the Pt/graphene composite. Ozone decomposition reactions are closely associated with the change of electronic state of Pt/graphene composite and the delocalization of the transfer electrons between the π orbitals of graphene and the d orbitals of metal atoms, which further verifies the synergetic effect of such metal/graphene composites. These investigations of the synergetic effect of the host−guest system can lead to new advances and applications pertaining to functional materials.

Acknowledgment. We are grateful for the financial support from the State Key Laboratory of Urban Water Resource and Environment, Harbin Institute of Technology (2010TS06).

References and Notes

(1) Geim, A. K.; Morozov, S. V.; Novoselov, K. S.; Geim, A. K.; Morozov, S. V.; Jiang, D.; Zhang, Y.; Dubonos, S. V.; Grigorieva, I. V.; Firsov, A. A. *Science* **2004**, *306*, 666.

(2) Tombros, N.; Jozsa, C.; Popinciuc, M.; Jonkman, H. T.; van Wees, B. J. *Nature* **2007**, *448*, 571.

(3) Novoselov, K. S.; Geim, A. K.; Morozov, S. V.; Jiang, D.; Katsnelson, M. I.; Grigorieva, I. V.; Dubonos, S. V.; Firsov, A. A. *Nature* **2005**, *438*, 197.

(4) Novoselov, K. S.; Jiang, D.; Zhang, Y.; Morozov, S. V.; Stormer, H. L.; Zeitler, U.; Maan, J. C.; Boebinger, G. S.; Kim, P.; Geim, A. K. *Science* **2007**, *315*, 1379.

(5) Liu, J.; Yin, Z.; Cao, X.; Zhao, F.; Ling, A.; Xie, L.; Fan, Q.; Boey, F.; Zhang, H.; Huang, W. *ACS Nano* **2010**, *4*, 3987.

(6) Liu, J.; Lin, Z.; Liu, T.; Yin, Z.; Zhou, X.; Chen, S.; Xie, L.; Boey, F.; Zhang, H.; Huang, W. *Small* **2010**, *6*, 1536.

(7) Tang, L. H.; Wang, Y.; Li, Y. M.; Feng, H. B.; Lu, J.; Li., J. H. *Adv. Funct. Mater.* **2009**, *19*, 2782.

(8) Castro Neto, A. H.; Guinea, F.; Peres, N. M. R.; Novoselov, K. S.; Geim, A. K. *Rev. Mod. Phys.* **2009**, *81*, 109.

(9) Schniepp, H. C.; Li, J. L.; McAllister, M. J.; Sai, H.; Herrera-Alonso, M.; Adamson, D. H.; Prud'homme, R. K.; Car, R.; Saville, D. A.; Aksay, I. A. *J. Phys. Chem. B* **2006**, *110*, 8535.

(10) McAllister, M. J.; Li, J. L.; Adamson, D. H.; Schniepp, H. C.; Abdala, A. A.; Liu, J.; Herrera-Alonso, M.; Milius, D. L.; Car, R.; Prud'homme, R. K.; Aksay, I. A. *Chem. Mater.* **2007**, *19*, 4396.

(11) Geim, A. K.; Novoselov, K. S. *Nat. Mater.* **2007**, *6*, 183.

(12) He, S. J.; Song, B.; Li, D.; Zhu, C. F.; Qi, W. P.; Wen, Y. Q.; Wang, L. H.; Song, S. P.; Fang, H. P.; Fan, C. H. *Adv. Funct. Mater.* **2010**, *20*, 453.

(13) Cao, Y.; Liu, S.; Shen, Q.; Yan, K.; Li, P. J.; Xu, J.; Yu, D. P.; Steigerwald, M. L.; Nuckolls, C.; Liu, Z. F.; Guo, X. F. *Adv. Funct. Mater.* **2009**, *19*, 2743.

(14) Wu, S.; Yin, Z.; He, Q.; Huang, X.; Zhou, X.; Zhang, H. *J. Phys. Chem. C* **2010**, *114*, 11816.

(15) Huang, X.; Zhou, X.; Wu, S.; Wei, Y.; Qi, X.; Zhang, J.; Boey, F.; Zhang, H. *Small* **2010**, *6*, 513–516.

(16) Qi, X.; Pu, K.; Zhou, X.; Li, H.; Liu, B.; Boey, F.; Huang, W.; Zhang, H. *Small* **2010**, *6*, 663.

(17) Morozov, S. V.; Novoselov, K. S.; Katsnelson, M. I.; Schedin, F.; Elias, D. C.; Jaszczak, J. A.; Geim, A. K. *Phys. Rev. Lett.* **2008**, *100*, 016602.

(18) Li, B.; Cao, X.; Ong, H. G.; Cheah, J. W.; Zhou, X.; Yin, Z.; Li, H.; Wang, J.; Boey, F.; Huang, W.; Zhang, H. *Adv. Mater.* **2010**, *22*, 3058.

(19) Bao, Q. L.; Zhang, H.; Wang, Y.; Ni, Z. H.; Yan, Y. L.; Shen, Z. X.; Loh, K. P.; Tang, D. Y. *Adv. Funct. Mater.* **2009**, *19*, 3077.

(20) Wang, X.; Zhi, L.; Mullen, K. *Nano Lett.* **2008**, *8*, 323.

(21) Yin, Z.; Wu, S.; Zhou, X.; Huang, X.; Zhang, Q.; Boey, F.; Zhang, H. *Small* **2010**, *6*, 307.

(22) Schedin, F.; Geim, A. K.; Morozov, S. V.; Hill, E. W.; Blake, P.; Katsnelson, M. I.; Novoselov, K. S. *Nat. Mater.* **2007**, *6*, 652.

(23) He, Q.; Sudibya, H. G.; Yin, Z.; Wu, S.; Li, H.; Boey, F.; Huang, W.; Chen, P.; Zhang, H. *ACS Nano* **2010**, *4*, 3201.

(24) Wang, Z.; Zhou, X.; Zhang, J.; Boey, F.; Zhang, H. *J. Phys. Chem. C* **2009**, *113*, 14071.

(25) Bunch, J. S.; Verbridge, S. S.; Alden, J. S.; van der Zande, A. M.; Parpia, J. M.; Craighead, H. G.; McEuen, P. *Nano Lett.* **2008**, *8*, 2458.

(26) Wehling, T. O.; Novoselov, K. S.; Morozov, S. V.; Vdovin, E. E.; Katsnelson, M. I.; Geim, A. K.; Lichtenstein, A. *Nano Lett.* **2008**, *8*, 173.

(27) Guo, S.; Dong, S.; Wang, E. *ACS Nano* **2010**, *4*, 547.

(28) Yoo, E. J.; Okata, T.; Akita, T.; Kohyama, M.; Nakamura, J.; Honma, I. *Nano Lett.* **2009**, *9*, 2255.

(29) Dong, L.; Gari, R. R. S.; Li, Z.; Craig, M. M.; Hou, S. *Carbon* **2010**, *48*, 781.

(30) Kou, R.; Shao, Y.; Wang, D.; Engelhard, M. H.; Kwak, J. H.; Wang, J.; Viswanathan, V. V.; Wang, C.; Lin, Y.; Wang, Y.; Aksay, I. A.; Liu, J. *Electrochem. Commun.* **2009**, *11*, 954.

(31) Watcharotone, S.; Dikin, D. A.; Stankovich, S.; Piner, R.; Jung, I.; Dommett, H. B.; Evmenenko, G.; Wu, S. E.; Chen, S. F.; Liu, C. P.; Nguyen, S. T.; Ruoff, R. S. *Nano Lett.* **2007**, *7*, 1888.

(32) Li, X.; Wang, X.; Zhang, L.; Lee, S.; Dai, H. *Science* **2008**, *319*, 1229.

(33) Si, Y.; Samulski, E. T. *Chem. Mater.* **2008**, *21*, 6792.

(34) Pasricha, R.; Gupta, S.; Srivastava, A. K. *Small* **2009**, *5*, 2253.

(35) Luechinger, N. A.; Athanassiou, E. K.; Stark, W. J. *Nanotechnology* **2008**, *19*, 445201.

(36) Kaniyoor, A.; Jafri, R. I.; Arockiadoss, T.; Ramaprabhu, S. *Nanoscale* **2009**, *1*, 382.

(37) Stankovich, S.; Dikin, D. A.; Dommett, G. H. B.; Kohlhaas, K. M.; Zimney, E. J.; Stach, E. A.; Piner, R. D.; Nguyen, S. T.; Ruoff, R. S. *Nature* **2006**, *442*, 282.

(38) Yu, A. P.; Ramesh, P.; Itkis, M. E.; Bekyarova, E.; Haddon, R. C. *J. Phys. Chem. C* **2007**, *111*, 7565.

(39) Williams, G.; Seger, B.; Kamat, P. V. *ACS Nano* **2008**, *2*, 1487.

(40) Lightcap, I. V.; Kosel, T. H.; Kamat, P. V. *Nano Lett.* **2010**, *10*, 577.

(41) Li, Y.; Tang, L.; Li, J. *Electrochem. Commun.* **2009**, *11*, 846.

(42) Yoo, E. J.; Okata, T.; Akita, T.; Kohyama, M.; Nakamura, J.; Honma, I. *Nano Lett.* **2009**, *9*, 2255.

(43) Kou, R.; Shao, Y.; Wang, D.; Engelhard, M. H.; Kwak, J. H.; Wang, J.; Viswanathan, V. V.; Wang, C.; Lin, Y.; Wang, Y.; Aksay, I. A.; Liu, J. *Electrochem. Commun.* **2009**, *11*, 954.

(44) Seger, B.; Kamat, P. V. *J. Phys. Chem. C* **2009**, *113*, 7990.

(45) Perdew, J. P.; Burke, K.; Ernzerhof, M. *Phys. Rev. Lett.* **1996**, *77*, 3865.

(46) Delley, B. *J. Chem. Phys.* **1990**, *92*, 508.

(47) Bratlie, K. M.; Lee, H.; Komvopoulos, K.; Yang, P.; Somorjai, G. A. *Nano Lett.* **2007**, *7*, 3097.

(48) Lee, H.; Habas, S. E.; Kweskin, S.; Butcher, D.; Somorjai, G. A.; Yang, P. D. *Angew. Chem., Int. Ed.* **2006**, *45*, 7824.

(49) Govind, N.; Petersen, M.; Fitzgerald, G.; King-Smith, D.; Andzelm, J. *Comput. Mater. Sci.* **2003**, *28*, 250.

(50) Pauling, L. *The Nature of the Chemical Bond*; Cornell University Press: New York, 1960.

(51) Sun, C. Q.; Wang, Y.; Nie, Y.; Sun, Y.; Pan, J.; Pan, L.; Sun, Z. *J. Phys. Chem. C* **2009**, *113*, 21889.

(52) Sun, Y.; Wang, Y.; Pan, J. S.; Wang, L. L.; Sun, C. Q. *J. Phys.Chem. C* **2009**, *113*, 14696.

(53) Sun, C. Q. *Phys. Rev. B* **2004**, *69*, 045105.

(54) Xia, W.; Li, J. H.; Weng, W. Z.; Wan, H. L. *Chem. Phys. Let.* **2006**, *423*, 427.

(55) Huang, X.; Zhai, H.; Waters, T.; Li, J.; Wang, L. *Angew. Chem., Int. Ed.* **2006**, *45*, 657.

JP1072523